Investigating the Neurological Immune Response to Moderate Dose of SARS-CoV-2 Infection in K18-hACE2 Transgenic Mouse Model

Anan Islam, May 2024

Director of Thesis: Dr. Jeffery B. Eells

Major Department: Brody School of Medicine, Department of Anatomy and Cell Biology

Abstract

Since the onset of the coronavirus pandemic, considerable research has been conducted to explore the impact of SARS-CoV-2 infection on the human immune system and the body. However, less attention has been given to investigating "long COVID," defined by the CDC as persisting symptoms lasting at least three months post-infection. Therefore, current research has focused on understanding the effects of SARS-CoV-2 infection on the brain's immune response and behavioral or cognitive functions.

Existing literature has proven angiotensin-converting enzyme 2 (ACE2) involvement in SARS-CoV-2 infection. Interestingly, this host entry receptor also plays a role in the upregulation of B1R expression associated with inflammation. Thus, our study aims to understand the benefit of oppressing the B1R during prolonged COVID-19 infection. Therefore, the hypothesis is that SARS-CoV-2 infection induces B1R expression in the brain, driving glial cell activation and cognitive and neuropsychiatric symptoms.

We used our lab-established long COVID mouse model to test our hypothesis, including the K18-hACE2 transgenic mouse model infected at $4x10^3$ TCID SARS-CoV-2. The design

involved testing with the B1R antagonist, SSR240612, in thirty-two mice divided appropriately into four groups evaluating glial cell activation, B1R expression, cognitive function, and behavior.

Our study observed a 10% increase in survival rates among groups infected with SARS-CoV-2 when treated with a B1R antagonist. Cognitive trends indicated that B1R antagonists protected against deficits induced by $4x10^3$ TCID50 dose. Our findings also support existing research indicating elevated B1R expression following SARS-CoV-2 infection. Furthermore, analysis of glial cells suggests activation during SARS-CoV-2 infection. These results indicate that the B1R Antagonist SSR240612 plays a role in glial cells' neurological and immune response to inflammation and changes in behavior induced by mild SARS-CoV-2 infection.

Investigating the Neurological Immune Response to Long Covid SARS-CoV-2 Infection in K18-hACE2 Transgenic Mouse Model

A Thesis

Presented to the Faculty of the Department of Anatomy and Cell Biology

East Carolina University

In Partial Fulfillment of the Requirements for the Degree

Master of Science in Biomedical Sciences with Concentration in Neuroscience

By

Anan Islam

May 2024

Director of Thesis: Jeffrey B. Eells, PhD

Thesis Committee Members:

Srinivas Sriramula, PhD

Shaw M. Akula, PhD

TABLE OF CONTENTS

LIST OF TABLES

LIST OF FIGURES

LIST OF ABBREVIATIONS

SARS-CoV	Severe Acute Respiratory Syndrome Coronavirus
CDC	Centers for Disease Control and Prevention
MERS-CoV	Middle East Respiratory Syndrome Coronavirus
WHO	World Health Organization
SARS-CoV-2	Severe Acute Respiratory Syndrome Coronavirus 2
PACS	Post-Acute COVID-19 Syndrome
PASC	Post-Acute Sequelae of SARS-CoV-2 Infection
ACE2	Angiotensin Converting Enzyme 2
TMPRSS2	Transmembrane Serine Protease 2
DABK	DES-ARG^{9}-Bradykinin
K18-hACE2	Human ACE2 Under Control of the Human Keratin 18 Promoter
B1R	Bradykinin B1 Receptor
TBI	Traumatic Brain Injury
B2R	Bradykinin B2 Receptor
IBA1	Ionized Calcium Binding Adaptor Molecule 1
BBB	Blood Brain Barrier
GFAP	Glial Fibrillary Acidic Protein
IACUC	Institutional Animal Care and Use Committee
IBC	Institutional Biosafety Committee
NIH	National Institutes of Health
DPI	Days Post Infection
dH_2O	Distilled Water
PBS	Phosphate Buffer Saline
BSA	Bovine Serum Albumin
SEM	Standard Error of Mean
HIV	Human Immunodeficiency Virus
BPA	Bracial Plexus Avulsion

1 CHAPTER 1: Introduction

1.1 SARS-CoV

Severe acute respiratory syndrome coronavirus (SARS-CoV) emerged in Asia in February 2003. Later, it spread to more than twenty-four countries on continents including North America, South America, Europe, and Asia before being contained. According to the Centers for Disease Control and Prevention (CDC), this epidemic accounted for a 10% mortality rate, with 812 deaths from a total of 8439 infected (1). Following this epidemic in 2012, Saudi Arabia experienced the emergence of the Middle East Respiratory Syndrome (MERS-CoV). This virus would spread to twenty-seven countries in the Middle East, Africa, and South Asia. According to the World Health Organization (WHO), 858 known deaths occurred because of the outbreak (2). In 2019, the novel severe acute respiratory syndrome coronavirus 2 (SARS-CoV-2) emerged in Asia. This prolific virus caused a global pandemic accounting for more than seven million deaths and more than seven hundred million cases (3). Thus, it has been well-documented how infection with SARS-CoV-2 can cause severe complications with organs such as the heart and the lungs (4); however, neurological manifestations have been investigated less. Clinical manifestations of SARS-CoV-2 infection vary in severity, ranging from asymptomatic to death (5).

1.2 Long-term Consequences of SARS-CoV-2 Infection

The current concern is that patients once infected with SARS-CoV-2 report symptoms persisting for many months. This concept of persistent symptoms has been coined as post-acute COVID-19 syndrome (PACS), post-acute sequelae of SARS-CoV-2 infection (PASC), or long COVID (6). The CDC defines long COVID as symptoms persisting for longer than three months after infection. Long COVID is suspected to impact one in three people who have been infected with SARS-CoV-2 (7). This includes individuals who are asymptomatic or have mild symptoms.

Individuals with mild symptoms have reported symptoms such as shortness of breath, 'brain fog,' headaches, chest pain, and unusual tiredness (8).

1.3 SARS-CoV-2 Spike Glycoprotein Tropism

SARS-CoV-2 comprises four structural proteins: a membrane protein, a nucleocapsid protein, an envelope protein, and a spike glycoprotein. However, the spike glycoprotein is the primary determinant of coronavirus tropism (9). The spike glycoprotein consists of two subunits denoted as S1 and S2. S1 binds to host entry receptors, specifically the angiotensin-converting enzyme 2 (ACE2). Then, S2 mediates the membrane fusion. After S1 binds to ACE2 on the target cell, the spike glycoprotein is then cleaved by the transmembrane serine protease 2 (TMPRSS2) at the S2 site. This cleavage activates the S2 subunit trimer to fuse to the host lipid bilayer, releasing the ribonucleoprotein complex into the cell.

1.4 SARS-CoV-2 Infection Influence on B1R Expression

Bradykinin-1 receptor (B1R) is a G-protein-coupled receptor that plays an essential role in mediating the effects of bradykinin, a peptide involved in inflammation. Normally, high-molecular-weight kallikrein will become bradykinin, which acts on Bradykinin B2 receptors (B2R). However, during SARS-CoV-2 infection, ACE2 receptors are disabled, facilitating the conversion into DABK. This results in elevated DABK levels that act on the B1R (Figure 2). Thus, increased B1R expression has been linked to heightened inflammation.

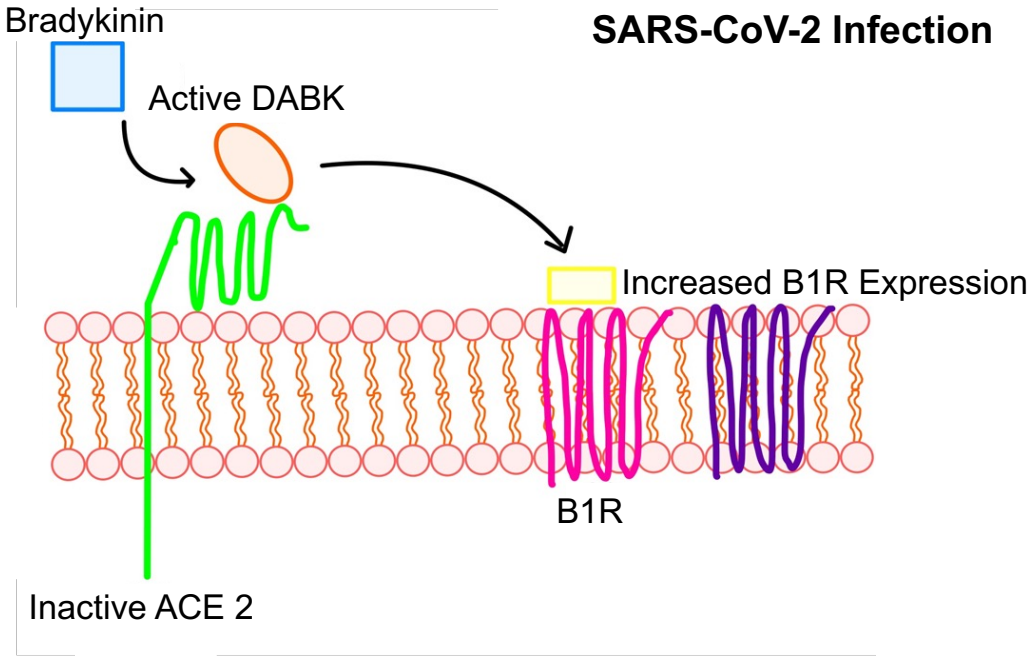

Figure 2. Hypothesized Mechanism of B1R Expression During SARS-CoV-2 Infection

1.5 B1R Expression and Neurological Immune Response

Pathogenesis of SARS-CoV-2 includes an increase in inflammation. It is imperative as various neurological manifestations have been identified clinically. A previous study compiled data on the prevalence of neurological manifestations with long COVID in four cohort studies. The results of this study indicated that 71% of patients infected with SARS-CoV-2 displayed neurological manifestations. These manifestations included myalgia, headache, impaired consciousness, stroke, or 'brain fog' (10). In the same study, SARS-CoV and MERS-CoV also had neurological implications in patients; however, the patient sample size for these groups was significantly smaller. The kallikrein-kinin system is implicated in the pathogenesis of inflammation. B1R mediates the system as it interacts with bradykinin metabolites, triggering a pro-inflammatory response (42). To assess this B1R expression in an inflammation model, a

study used traumatic brain injury (TBI) to see if inflammation influenced neurobehavioral evaluations. The study found that although B1R and bradykinin B2 receptor expression was higher after one week, the B1R expression was the only significant receptor expression (11). Despite this, the literature has not explicitly examined the role of B1R during SARS-CoV-2.

1.6 Glial Cell Activation

Neuroinflammation is characterized by the activation of glial cells, which are responsible for the development of neurodegeneration by releasing inflammatory mediators (43). When assessed in human neurodegenerative disorders, glial cells can change morphology, function, and abundance (14). Glial cells, in particular, microglia and astrocytes, serve a variety of tasks that include innate immune responses by having phenotypes that are either neuroprotective or neurotoxic (13). Microglia first respond to pathological attacks, maintaining homeostasis and host defense mechanisms (15). Ionized calcium-binding adaptor molecule 1(IBA1) can be the known marker for microglia activation; however, it cannot distinguish between distinct activation types (20). Thus, observing microglia with a smaller cell area and fewer skeleton branches would indicate an activated microglia morphology (21). Astrocytes are the most common glial cells in the brain responsible for various functions that regulate homeostasis (16-17). This includes maintaining the blood-brain barrier (BBB), regulating blood flow, scar formation, ion balance, and managing synaptic activity (18-19). Glial fibrillary acidic protein (GFAP) can be used for blood biomarkers; thus, by looking at increasing branch length, it is possible to determine an activated astrocyte morphology (22-23).

1.7 Behavioral and Cognitive Function

Individuals with long COVID have reported behavioral and cognitive function deficits such as symptoms of “brain fog,” neuralgia, anxiety, and depression. Individuals who list ‘brain

fog' as one of their symptoms would be expected to struggle with recalling information (8). Thus, spatial working memory becomes a vital component in understanding cognitive function. Due to this, the hippocampal area becomes the brain region of interest as it plays a crucial role in spatial working memory (24). To quantify the changes in cognitive function, using a Y-maze test to obtain percent spontaneous alternation is advantageous, as it is the primary test for spatial working memory (25). Earlier research in our lab could not conclude statistically significant results in the percent spontaneous alternation between infected and control groups (12). SARS-CoV-2 infection has also been linked to anxiety (26). Interestingly, neuroinflammation could be found to cause alterations in the structure or function of anxiety-related brain circuits, including areas such as the prefrontal cortex (27). Previous research in our lab has indicated elevated levels of anxiety in mice infected with SARS-CoV-2 utilizing a zero-maze test (12). Lastly, overall exploration and behavior is a measure of interest. Previous research has used the open field to measure changes in various behaviors, such as rearing, grooming, and overall exploration (12,28).

1.8 K18-hACE2 Transgenic Mouse Model

Various COVID-19 mouse models have been established. The hACE2 transgenic mouse model mimics human-like viral entry by efficiently assessing SARS-CoV-2 infection; however, it limits the ability to study interactions unrelated to ACE2. TMPRSS2 transgenic mice investigate the role of TMPRSS2 in pathogenesis. This mouse model overexpresses the serine protease and limits studies to assess TMPRSS2-related mechanisms. Another mouse model that provides an authentic SARS-CoV-2 infection model is hACE2 knock-in mice. These mice have replaced the ACE2 with a human ACE2; however, there is a variability in expression levels when observing various tissues. Previously, our lab utilized a subset of hACE2 transgenic mice expressing human ACE2 under the control of the human keratin eighteen promoter (K18-hACE2 mice), which is widely used as a laboratory animal model suitable for studying long COVID pathogenesis (12). By looking at the survival post-infection for both low and high-dose groups, the high dose causes all mice to die by day seven. Although the low dose impacts the groups,

mice recover after day nine. To evaluate for long-term COVID-19, a mild form of the disease has been found effective at a dose of $4x10^3$ TCID50 SARS-CoV-2. This dose had an 80% mice survival rate. No significant differences were seen between sexes for change in percent body weight, and infection was confirmed by detecting antibody titers in infected groups being higher than that of the control groups.

1.9 Main Hypothesis & Specific Aims

Based on the literature and previous studies in our laboratory relating B1R activation and long-term COVID, I formulated the hypothesis: SARS-CoV-2 infection induces B1R expression in the brain, driving glial cell activation and, ultimately, cognitive and neuropsychiatric symptoms.

Therefore, the aims of this project are:

AIM 1: Determine if B1R antagonism in a mild SARS-CoV-2 infection will increase glial cell activation.

AIM 2: Determine the impact of B1R antagonism in a mild SARS-CoV-2 infection on spatial working memory, anxiety levels, and exploratory behavior.

2 CHAPTER 2: Materials and Methods

2.1 Study Approval

The study got approval by the Institutional Animal Care and Use Committee (IACUC) protocol (AUP #A209) at East Carolina University (AAALAC-accredited facility, Animal welfare assurance number A3469-01). The Institutional Biosafety Committee (IBC) approved using the SARS-COV-2 strain under BSL3 conditions in an AALAC-accredited facility by certified staff. Procedures were to follow basic guidelines in the National Institutes of Health (NIH) Guide for the Care and Use of Laboratory Animals. IBC-approved standard operating procedures for removing specimens from high containment were used for all sample inactivation.

2.2 SARS-CoV-2 Virus

Work involving the use of SARS-CoV-2 was performed in a BSL-3 laboratory. SARS-CoV-2 (isolate USA-WA1/2020) was purchased from BEI Resources (Manassas, VA, USA). It was propagated, purified, and titrated in Vero cells per the standard protocols (44).

2.3 Experimental Design

The study consisted of thirty-two transgenic mice with the human ACE2 gene under the control of K18 promoter (B6.Cg-Tg(K18-ACE2)2Primn/J, Jackson Labs, Strain #034860), which were divided into four groups (mock, SARS-CoV-2, SSR240612, SARS-CoV-2 + SSR240612). The mice used included males and females between 3 to 4 months old. The body weight distribution of male mice was observed within the range of 30 to 40 grams, while female mice exhibited body weights falling within the range of 20 to 30 grams. The mice were randomly assigned to the following experimental groups: mock (n=6), SSR240612 (n=6), SARS-CoV-2 (n=10), and SARS-CoV-2 + SSR240612 (n=10). Mice that received the virus did so at a 4×10^3 tissue culture infectivity dose (TCID50) SARS-CoV-2, while those that did not receive saline as

a control. Similarly, mice who received the B1R antagonist, SSR240612, did so at a dose of 5-10 mg/kg/day, while those who did not received 40% DMSO/60% saline as a control.

To ensure that the B1R antagonist was effective by the day of infection (Day 0), all mice groups were implanted with an osmotic pump two days before day zero. The pump would deliver 0.11 uL/h of SSR240612 at a dose of 15mg/kg/day for 28 days for drug groups and 40% DMSO/ 60% saline for vehicle groups. Mice were anesthetized with 3-4% isoflurane, and 12.5 uL of either vehicle or moderate dose SARS-CoV-2 was pipetted into each naris (25uL total volume). Following intranasal infection, mice were housed individually and managed in a BSL3 facility (East Carolina University, Greenville, NC). Each mouse was weighed daily for thirteen days post-infection (DPI). Mice that displayed symptoms of rapid weight loss or became moribund during the 13 days were euthanized. Additional body weights were taken on 20 dpi and 28 dpi. Behavioral and cognitive function tests began at 26 dpi and continued until 28 dpi. All remaining mice were euthanized at 30 dpi.

2.4 Behavioral and Cognitive Function Testing

At 26 dpi, behavior in mice began being evaluated and continued until 28 dpi. All testing was performed between 1300 and 1600 h, and all mice in treatment groups were assessed evenly throughout the testing time. Behavior apparatuses were encased in a Duo-Flo^{TM} mobile unit with BioClean^{TM} clean room technology. The lighting in the room was LED, which produced approximately one hundred lux of illumination. Once the behavior was recorded, EthoVision software was used to track mice movements. For the open field test, mice were initially placed in the center of the open field chamber (Stoelting open field, 40 cm x 40 cm, clear plexiglass). Each mouse was recorded for ten minutes. Mice were observed in an open field test to examine factors such as exploration and stress. This was done by looking at the parameters of total distance

traveled and rearing and grooming behavior. To assess anxiety, a Stoelting mouse zero maze was used. The diameter of the circular stage was 50 cm with 5 cm lanes and an adjustable rim at 3 mm. The mice were initially placed in the closed portion of the maze and recorded for ten minutes. Time spent in open regions was found by using EthoVision software to manually score for total time in the open area (defined as any part of the mouse entering the open region of the maze) and total time in the closed region (defined as any part of the mouse entering the closed area of the maze). Lastly, a Stoelting Y maze for mice was used with lanes 5 cm wide and a width of 35 cm in arm length. Each mouse was placed in the same arm of the Y maze and allowed to explore freely for five minutes. Each mouse was recorded and later analyzed using EthoVision software. A zone for each arm was made, and a center zone was extended 2.5 cm into each arm. Arm entries were only considered if the center point of the mouse crossed from the center zone into the respective arms labeled either “A,” “B,” or “C.” The number of entries was manually counted with the assistance of the EthoVision software. Also, spontaneous alternation was calculated to assess correct subsequent arm entries. It was defined as entries into three different arms consecutively (ABC, BCA, or CAB). Total arm entries would also be used as another marker for explorative behavior. All behavioral measurements were blinded to treatment and control groups. After each test, the mazes were cleaned with 70% isopropyl alcohol.

2.5 Brain Tissue Collection

At the end of the experimental protocol, mice were deeply anesthetized using isoflurane (4%) in an oxygen flow (1 L/min) and euthanized by decapitation. The thoracic cavity was then opened, and the heart was transcardially perfused with PBS, followed by paraformaldehyde (3%). Afterward, the brain was obtained, placed in a 15 mL conical tube, and later post-fixed in paraformaldehyde (3%). Using a sterile blade, each brain tissue was cut at -0.94mm Bregma and -2.70mm Bregma to preserve structures in the hippocampus region.

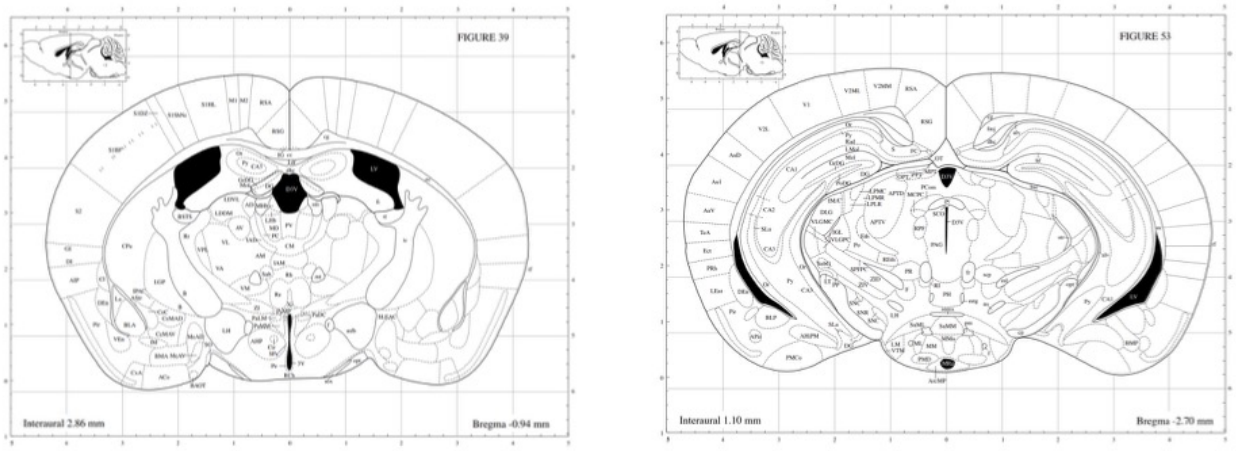

Figure 3. Brain Atlas Images of Sagittal Plane Sections of Hippocampus Region

2.6 Tissue Sectioning Procedure

Once brain tissue was cut to ensure structures in the hippocampus were preserved, it was then placed in varying concentrations of ethanol for 1 hour each. First, 70% ethanol, then 80% ethanol, then 95% ethanol two times, and finally 100% ethanol thrice. The tissue was placed in three successions of xylene for an hour each and finally placed in four successions of paraplast plus for an hour each. Once paraffin embedding was complete, one set of ten slides containing three ten-micron sagittal brain sections was obtained by using a microtome. This was done by placing the newly cut sections into ethanol and then transferring them into a 40-degree Celsius

water bath for thirty to forty-five minutes. The lack of wrinkles in the sections indicated that the tissue was ready to be placed on the glass slides. Once sections were prepared, they would be placed one at a time on a different glass slide (1-10) in ascending order so that each slide contained sections from other brain regions. The three sections on each slide were 100-micron intervals apart. Once complete, the sections were placed on a heated plate to dry.

2.7 Immunohistochemistry (Microglia, Astrocytes, B1R, Dapi)

After sections were prepared for immunohistochemistry, the slides underwent a deparaffinization process involving several steps. Initially, they were immersed in Xylazine for two consecutive steps, each lasting five minutes. Subsequently, the slides were exposed to 100% ethanol for two steps, each lasting five minutes, followed by 95% ethanol for five minutes each. The following steps involved 80% ethanol for three minutes and a final immersion in distilled water (dH_20) for three minutes.

Once the deparaffinizing step was complete, the antigen retrieval step was performed by immersing slides in a beaker with ten mM citrate solution. The solution was heated to one hundred degrees Celsius on a hot plate and was continuously mixed with a stir bar set to 100 rpm. As the solution evaporated, dH20 was occasionally added to keep liquid levels constant. After twenty minutes, the beaker was taken off the hot plate and allowed to cool for thirty minutes. The slides were rinsed with 1X phosphate buffer saline (PBS) for three minutes. A hydrophobic pen was then used to enclose the tissue samples before incubating them with a blocking buffer. 4% normal goat serum in 1X PBS, 0.1% Triton-X, and 1% bovine serum albumin (BSA). 250 uL blocking buffer was added to each slide and incubated at 4 degrees Celsius for twenty minutes in a slide humidity incubation box. After twenty minutes of incubation with a blocking buffer, a primary antibody stain was added. The antibody was diluted

in 1X PBS, 0.1% Triton-X, 1% BSA solution, and then 250 uL of primary antibody solution was added to each slide and incubated overnight at 4 degrees Celsius.

After the primary antibody incubation period, slides were rinsed twice for five minutes each in 1X PBS and 1% BSA solution. 250 uL of the secondary antibody diluted in 1X PBS, 0.1% Triton-X, and 1% BSA was added to each slide and incubated at room temperature in a slide humidity incubation box for two hours. After the secondary antibody incubation step, slides were rinsed thrice for five minutes with 1X PBS and 1% BSA. 250 uL of 500 nM of data are added to each slide and incubated at room temperature for twenty minutes. Slides are rinsed twice for five minutes in 1X PBS and 1% BSA. Finally, slides are mounted with mounting media and placed on a dry slide humidity incubation box.

Images of the hippocampus were taken of sagittal brain sections using a Keyence microscope. Settings on the microscope used for microglia and astrocyte imaging included "20X" for the lens, "excitation light" for illumination, "mono" for the camera, "auto" for exposure, and "auto-focus" for z position. Settings on the microscope used for B1R imaging included: "40X" for lens, "excitation light" for illumination, "mono" for camera, "1/2.5s" for exposure, and "auto-focus" for z position. Settings on the microscope used for dapi imaging included: "40X" for lens, "excitation light" for illumination, "mono" for camera, "1/40s" for exposure, and "auto-focus" for z position. The stitching feature combined images to obtain a cohesive picture of the entire hippocampus region.

2.8 Glial Cell Immunohistochemistry Analysis

Image J was used to analyze glial cells in the hippocampal region of five mice per group. Channels split 20X images of the hippocampus region, and only the green channel was kept for GFAP staining, and the red channel was kept for Iba1 staining. The image was then changed to

display greys. The image process added a bandpass filter with settings for filtering large structures down to forty pixels, filtering small structures up to three pixels, having no suppress stripes, and having a 5% tolerance of direction. The image would then be "auto" adjusted for brightness and color and followed by adding an unsharp mask filter with settings of a radius (Sigma) of 3.0 pixels and a mask weight of 0.60. The process would then reduce noise by "despeckle," Image was then adjusted for threshold with settings of "auto" threshold, "Default" and "B&W" selected, and dark background unselected. "Despeckle" was used again, followed by "close," and then removed of outliers. The outliers removed had settings of a 2.0-pixel radius and threshold of fifty. Once complete, the image was saved and ready to be skeletonized using the plugin "Skeletonize." Once skeletonized images of glial cells appeared glial cells were then numbered, and then ten glial cells were randomly selected for skeleton analysis. A total of two hundred data points would be obtained with fifty skeleton analysis results for each group.

2.9 Bradykinin-1 Receptor Immunohistochemistry Analysis

Image J was used to analyze B1R expression from the hippocampal region of five mice in each group. 40X magnification images were split by image channel, and only the red channel was kept. A scale was set using the scalebar obtained from imaging on the Keyence microscope. The "Macros" plugin on Image J/Fiji software was utilized to run a procedure on all images to measure expression quantification. Twenty data points would be obtained with five quantified B1R expressions belonging to each group.

Antibody	#	Dilution	Buffer
B1R	Alomone ABR 011	1:500 (overnight)	1x PBS, 1% BSA, 0.1% Triton-X
GFAP	Invitrogen 53 9892 82	1:500 (2 hours)	1x PBS, 1% BSA, 0.1% Triton-X
Iba1	WAKO 011-27991	1:500 (overnight)	1x PBS, 1% BSA, 0.1% Triton-X

Table 1. Primary Antibodies used with Reference Number, Dilution, and Buffer

2.10 Statistical Analysis

Statistical analysis was performed using Prism™ version 10.0 (GraphPad Software Inc., La Jolla, CA, United States). Results are expressed as the mean ± standard error of the mean (SEM)—one-way ANOVA, followed by Tukey's multiple comparisons test, which allowed for various comparisons. Results were considered significant at a value of $P<0.05$.

3 Chapter 3: Results

3.1 Mild Dose (4 x 10^3 TCID 50) of SARS-CoV-2 Induces Moderate Infection

We intranasally infected groups with either the moderate dose or saline to determine the effects of SARS-CoV-2 (4 x 10^3 TCID50) in K18-hACE2 transgenic mice, we intranasally infected groups with either the moderate dose or saline (control). Similarly, we desired to assess the effects of the B1R antagonist, SSR240612, in K18-hACE2 transgenic mice by placing an osmotic pump subcutaneously that released 0.11 uL/h of SSR240612 at a dose of 15mg/kg/day for 28 days for drug groups and 40% DMSO/ 60% saline for vehicle groups (Figure 4).

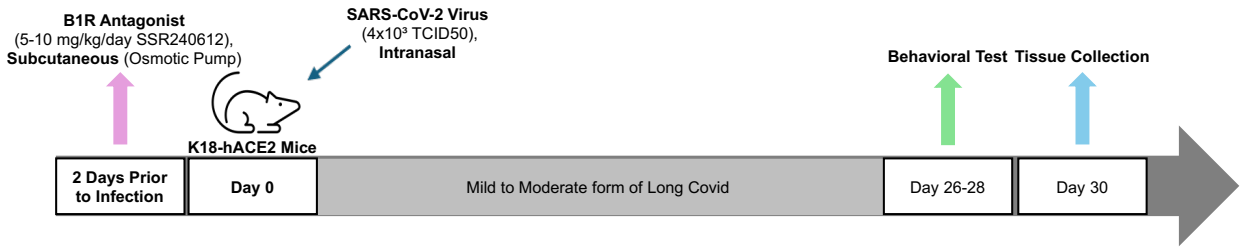

Figure 4. Mild dose of SARS-CoV-2 test against B1R antagonist. K18-hACE2 transgenic mice were either given B1R Antagonist, SSR240612 or 40% DMSO/60% saline (vehicle) by osmotic pump subcutaneously two days prior to infection. Mice were either infected with moderate dose 4 x 10^3 TCID50 or saline(control).

Animals were observed daily for changes in body weight and symptoms. Mice that had a rapid loss of body weight or became moribund before 13 dpi were euthanized. 20% of mice in the SARS-CoV-2 infection/vehicle group died by ten dpi, while 10% of mice in SARS-CoV-2/SSR240612 died by 11 dpi (Figure 5A). Of the thirty-two mice that participated in the experiment, only three experimental mice were euthanized before the completion of the experiment. They presented significant body weight changes, with almost 20% body weight decrease compared to their initial starting weight. However, all other SARS-CoV-2 mice began

experiencing recovery by increasing body weight percent after ten dpi (Figure 5B). All control mice made it to the completion of the experiment without presenting declining symptoms.

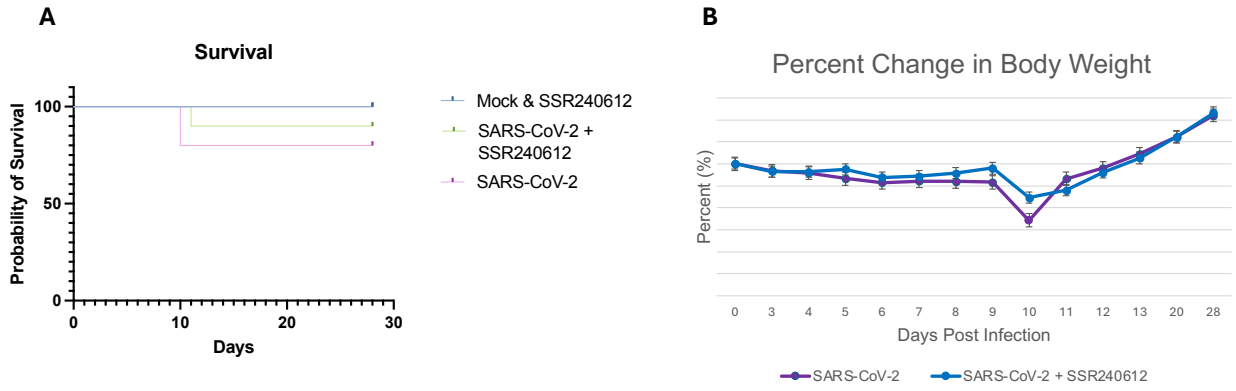

Figure 5. SARS-CoV-2 Infection induced differences in survival and percent body weight. (A) SARS-CoV-2 infection caused and effect in survival with 80% survival in SARS-CoV-2 infection/vehicle group and 90% survival in SARS-CoV-2 infection/SSR240612 group. (B) Recovery was seen in both groups 10 dpi with increasing body weight percentages.

3.2 B1R Antagonism Increased Exploration and Working Memory

On 26 dpi mice engaged in a Y maze test. Each mouse was initially placed in the same arm, "A," of a Stoelting Y maze and allowed to travel freely for five minutes. Their movements were recorded and later analyzed using EthoVision software. To determine the number of different arm entries, the maze had specific parameters that were identified, such as the center zone, and each arm was denoted as either "A," "B," or "C." Using the EthoVision software, a heat map of mice movement and the number of arm entries were acquired. No differences between groups were found in heat map quantifications for Y-maze (Figure 9B). Arm entries were recorded by manually scoring the mouse in a specific arm after the mouse's center point had crossed the maze's center zone into an arm. Groups with B1R antagonists had more arm entries than vehicle groups (Figure 6A). Mice belonging to the SSR240612 and SARS-CoV-2 + SSR240612 groups had the most arm entries, with an average of 19.0 ± 2.0 standard error of the

mean (SEM) and 20.0 ± 1.8 SEM arm entries, respectively. Mice in the mock and SARS-CoV-2 groups had the fewest arm entries, averaging 16.8 ± 2.3 SEM and 14.0 ± 1.4 SEM arm entries, respectively. Despite the exciting trend, after running one-way ANOVA on these findings, although not statistically significant, there was a solid trend (p=0.0526). However, utilizing Tukey's multiple comparison tests showed a significant difference in means between the SARS-CoV-2 and the SARS-CoV-2 + SSR240612 group (p=0.0440).

Percent spontaneous alternation was another aspect that was analyzed from mice groups. Assessing if a mouse could correctly enter three subsequent arm entries (ABC, BCA, or CAB) would be deemed a correct response. Results indicated that the SSR240612 group produced a higher percent spontaneous alternation than the SARS-CoV-2 group (Figure 6B). The SSR240612 group had the highest percent spontaneous alternation at 71.7% ± 6.1 SEM. At the same time, SARS-CoV-2 had the lowest percent spontaneous alternation at 48.7% ± 7.9 SEM. Interestingly, the one-way ANOVA statistical method displayed a lack of significance (p=0.1371) in this data at an alpha of 0.05. Despite not finding a significant difference in means between SARS-CoV-2 and SARS-CoV-2 + SSR240612 groups via Tukey's multiple comparison test, there was a similar trend in improved percent spontaneous alternation seen in arm entries.

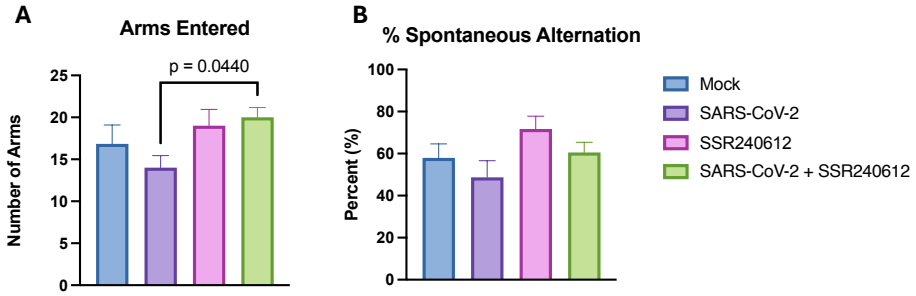

Figure 6. B1R Antagonism presented protective effects to SARS-CoV-2 infection. (A)B1R protected exploratory behavior in SARS-CoV-2 infected mice. (B)No significant differences were found in percent spontaneous alternation.

3.3 SARS-CoV-2 Infection Induces Anxiety

On 27 dpi all surviving mice participated in the zero-maze to evaluate for anxiety. This was done by placing each mouse in a Stoelting mouse zero maze for 10 minutes. Their movements were recorded and analyzed using EthoVision software. Using EthoVision software, we manually scored when the mouse went from a closed region to an open one. Total time in the open region (defined as any part of the mouse entering the open region of the maze) and total time in the closed region (defined as any part of the mouse entering the closed region of the maze) were calculated using these results. The group with SARS-CoV-2 spent the most time in the closed areas with an average of 286.0s ± 33.5 SEM, while the group receiving the SSR240612 spent the least amount of time in the closed region with an average of 153.5s ± 33.0 SEM (Figure 7A). The results of one-way ANOVA indicated no statistical significance (p=0.2355) for an alpha of 0.05. Despite this, mice receiving the SARS-CoV-2 alone spent the most amount of time in open regions with an average of 69.6s ± 15.7 SEM, while the SSR240612 alone group spent the least with an average of 33.5 ± 7.4 SEM (Figure 7B). The results of one-way ANOVA indicated no statistical significance (p=0.1117) for an alpha of 0.05.

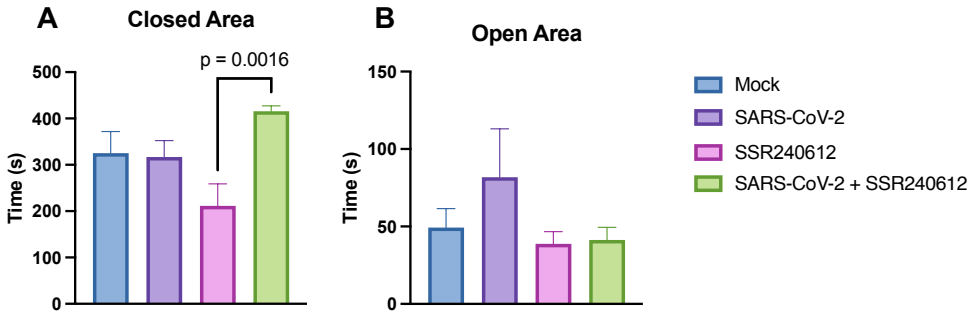

Figure 7. SARS-CoV-2 infection did not influence anxiety in transgenic K18-hACE2 mice. (A)Results indicated SARS-CoV-2 infection increased time spent in closed areas despite lacking significance. (B) No significant differences can be concluded from time spent in open regions of zero maze between groups.

3.4 SARS-CoV-2 + SSR240612 Groups Experienced Increased Exploration

On 28 dpi, mice were subjected to an open field test using a Stoelting open field, 40 cm x 40 cm, clear plexiglass container. Each mouse was placed in the center of the open field and recorded for ten minutes. Recordings were later analyzed using EthoVision software to obtain a heat map of mice movements and look at rearing (behavior defined as standing on hind legs), grooming, and total distance traveled. The generated heat map showed no distinct differences (Figure 9C). Assessment of rearing behavior indicates no significant differences ($p=0.8421$) amongst groups with similar average occurrences performing rearing behavior utilizing a one-way ANOVA with an alpha of 0.05 (Figure 8A).

Similarly, grooming behavior indicated no significant differences ($p=0.6315$) between groups with similar average occurrences performing grooming behavior (Figure 8B). Exploration was assessed using findings from the total distance traveled. It was found that the combo group traveled the furthest distance with an average of 3850.0cm ± 52.7 SEM, while the SSR240612 group traveled the least with an average distance of 2690cm ± 105.8 SEM (Figure 8B). The one-way ANOVA statistical method confirmed this by finding statistical significance ($p<0.0001$) at an alpha 0.05. After running Tukey's multiple comparison tests, it is possible to see there was a significant difference in means between SARS-CoV-2 and SARS-CoV-2 infection + SSR240612 groups.

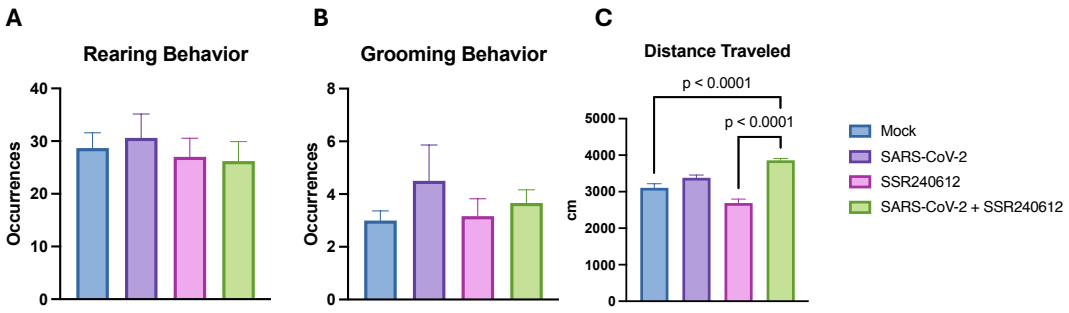

Figure 8. Increased exploration in infected mice treated with SSR240612. (A)No differences were seen between groups in rearing behavior. (B)No differences in grooming behavior were seen between groups. (C)Mice in SARS=CoV-2 infection groups regardless of treated with SSR240612 or vehicle explored more than sham infected groups.

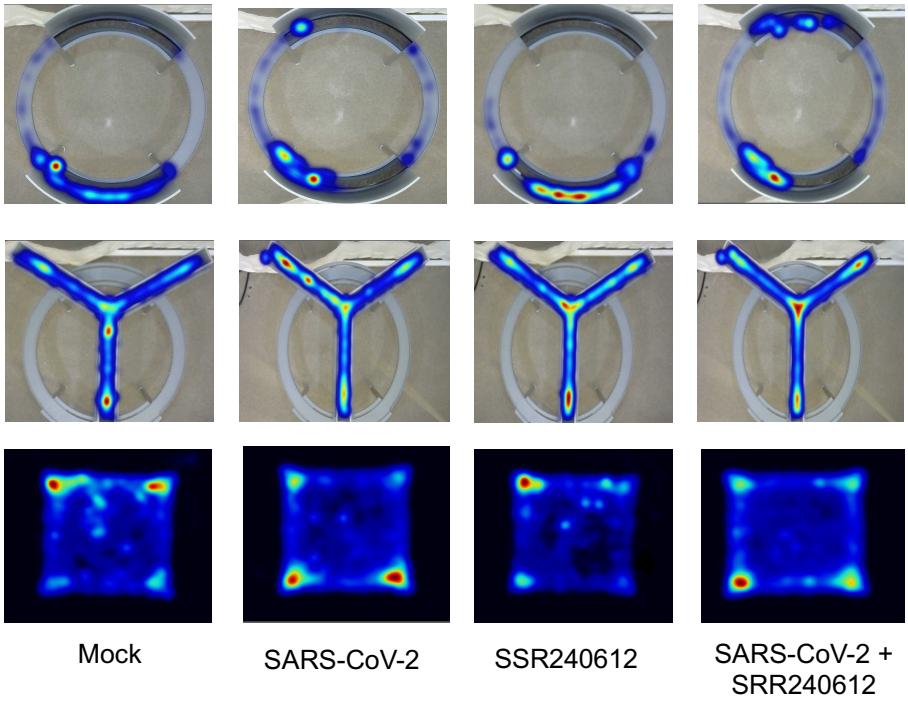

Figure 9. Mild SARS-CoV-2 infection causes neuropsychiatric symptoms. (A)No differences were seen between groups in zero maze heat map. (B)Heat map quantification supported B1R antagonism protective effects in arm entries between virus alone and combo groups. (C) Heat map quantification supported increase in distance traveled between mock and combo groups.

3.5 SARS-CoV-2 Infection Decreases Glial Cell Branching

Image J/Fiji software was used following the skeleton analysis protocol to obtain results regarding glial cell branching. Mice in the SARS-CoV-2 infected group had less microglia branching than sham groups (Figure 10A). Mice in the sham group, which also received

SSR240612, B1R antagonist, had the most branching compared to all other groups, with an average of 11.6 branches ± 1.4 SEM. These findings were statistically significant ($p<0.0001$) when a one-way ANOVA statistical method was compared against an alpha 0.05. Average branch length was found to be longest in the group infected with SARS-CoV-2 dose and vehicle with an average branch length of 0.47 um ± 0.05 SEM; however, average branch length was found to be the shortest in the group infected with SARS-CoV-2 dose and SSR240612 with an average branch length of 0.26 um ± 0.02 SEM (Figure 10B). These findings were statistically significant ($p=0.0001$) using a one-way ANOVA statistical method with an alpha 0.05.

Similarly, SARS-CoV-2 infected groups experienced decreased branching in astrocytes compared to other groups (Figure 10C). In particular, the SARS-CoV-2 infected group with the B1R antagonist, SSR240612, had the most branching with an average number of 7.7 branches at 0.7 SEM. These findings were statistically significant ($p<0.0001$) using a one-way ANOVA at an alpha 0.05. Astrocyte average branching length was found to be the longest in the SARS-CoV-2 infected group with the vehicle with an average branch length of 0.45 um ± 0.04 SEM and shortest in the SARS-CoV-2 infected group with B1R antagonist, SSR240612 with an average branch 0.23um ± 0.02 SEM (Figure 10D). Using a one-way ANOVA, these findings were statistically significant ($p<0.0001$) against an alpha 0.05.

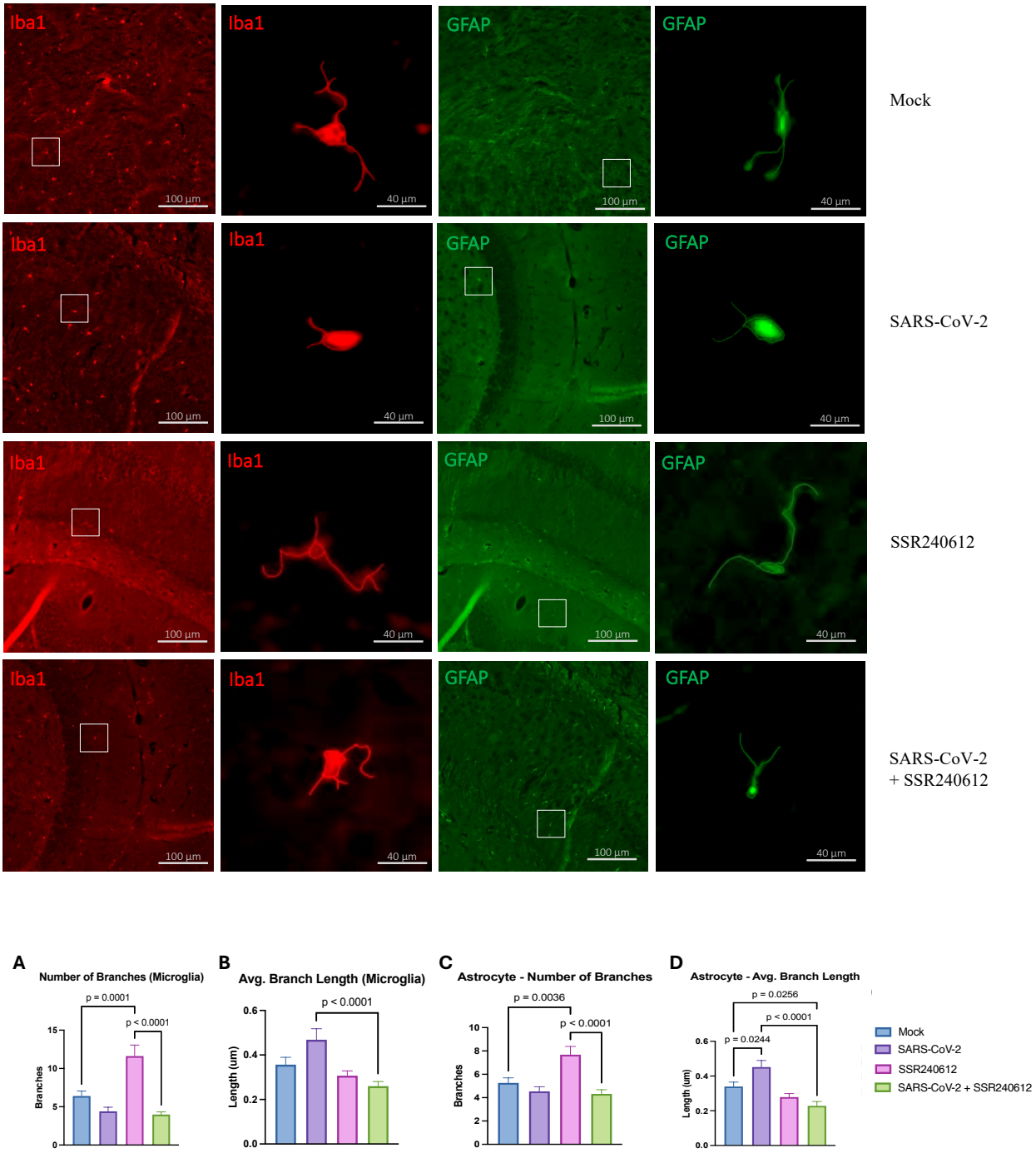

Figure 10. SARS-CoV-2 infection decreases glial cell branching, (A)Mice belonging to the sham and B1R antagonist group had the most amount of branching, while SARS-CoV-2 infected groups had the fewest branches in microglia. (B) Despite having fewer branches, microglia from SARS-CoV-2 infected and vehicle group had the longest average branch length. (C)Mice belonging to the sham and B1R antagonist group had the most amount of branching, while SARS-CoV-2 infected groups had the fewest branches in astrocytes. (D) Despite having fewer branches, astrocytes from SARS-CoV-2 infected and vehicle group had the longest average branch length.

3.6 SARS-CoV-2 Infection Increases B1R Expression

Image J/Fiji software was used to analyze receptor expression. SARS-CoV-2 infection groups had higher B1R expression than sham groups, and the B1R antagonist displayed an inhibiting effect (Figure 11). The SARS-CoV-2 infected/vehicle group had the highest B1R expression, with an average expression of 104.2 ± 16.8 SEM, and the sham with B1R antagonist group had the lowest B1R expression, with an average expression of 66.7 ± 2.8 SEM. These findings were statistically significant (p=0.0448) using a one-way ANOVA at an alpha 0.05.

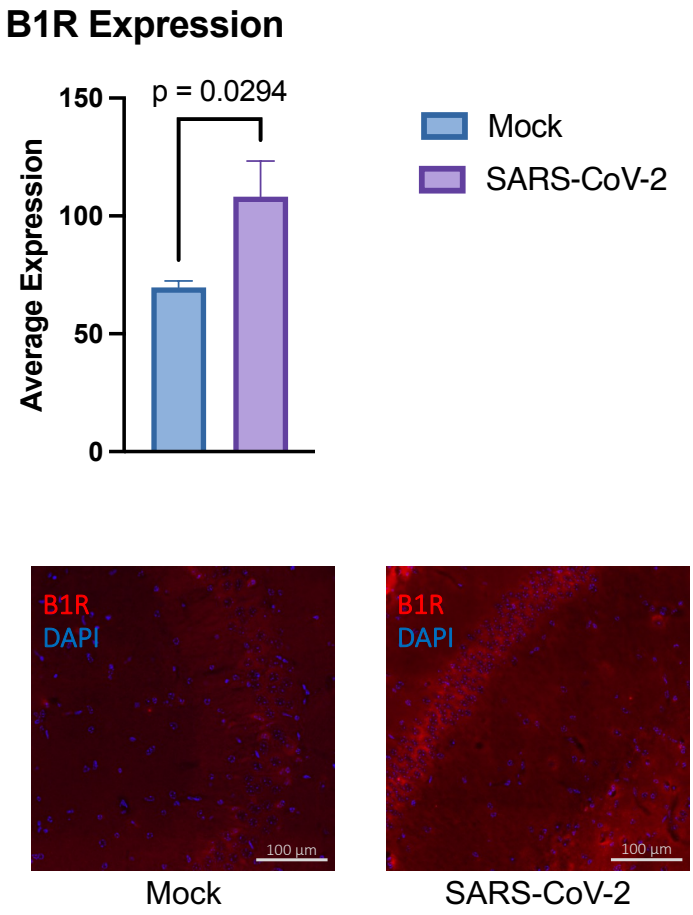

Figure 11. SARS-CoV-2 infection increases B1R expression. Mice in SARS-CoV-2 infected groups had higher B1R expression than mice in control (sham).

4 Chapter 4: Discussion

4.1 Study Summary

Our study aims to understand the impact of B1R antagonism on moderate SARS-CoV-2 infections by examining neuroinflammation and cognitive function. We achieved this by evaluating the neurological, immune response to a mild dose of SARS-CoV-2 in a K18-hACE2 transgenic mouse model. Specifically, we administered an intranasal 4 x 10^3 TCID50 of SARS-CoV-2. To investigate the effect of B1R antagonism before infection, we administered SSR240612, a B1R antagonist, to select groups of K18-hACE2 transgenic mice two days before infection. This extended COVID model in K18-hACE2 mice has previously been shown to have lung damage, elevated neuroinflammation, and cognitive/neuropsychiatric symptoms (35). The study spanned thirty days, during which three behavioral tests were conducted at the study's conclusion. While this model may not precisely replicate clinical long COVID, it is valuable for gaining mechanistic insights and establishing proof of concept.

4.2 SSR240612 Improves Survival of $4x10^3$ TCID50 dosed K18-hACE2 Mice

Our study validated the representative nature of the moderate SARS-CoV-2 dose (4x10^3 TCID50), consistent with findings from our laboratory's previously published work, demonstrating an 80% survival rate in the moderate dose group (12). In this current study, we observed a similar 80% survival rate in both the virus-alone group and a 90% survival rate in the combo group through survival analysis (Figure 5A). As expected, both sham virus control groups exhibited 100% survival. These results suggest that the 4x10^3 TCID50 SARS-CoV-2 dose is suitable for inducing moderate infection, as evidenced by the percentage increase in body weight after ten dpi (Figure 5B). Although not statistically significant due to the sample size, our findings suggest a potential protective effect of B1R antagonism, as evidenced by a 10%

improvement in survival from the SARS-CoV-2 infected/vehicle group to the SARS-CoV-2 infected/SSR240612 group. Previous research has discovered that a cellular inhibitor of TMPRSS2 can block the ACE2 receptor, which is responsible for the host cell entry of SARS-CoV-2, leading to improved survival (28). Thus, given what we know about coronavirus tropism, antagonism of the B1R may have a similar effect on survival. The decrease in inflammation due to antagonizing the B1R is potentially the reason behind the increased survival in the infected B1R antagonist group.

4.3 SSR240612 Combats Loss of Exploratory Behavior Induced by SARS-CoV-2 Infection

Twenty-nine mice completed the study and were subjected to cognitive testing. The Y-maze was used to assess changes in exploration and spatial working memory (25). During the Y-maze test, mice were allowed to move freely for 5 minutes to enter a new arm each time, which could be quantified as percent spontaneous alternation. One-way ANOVA analysis for total arm entries indicated no significant difference; however, Tukey's multiple comparisons test revealed a significant difference ($p=0.0440$) in means between the SARS-CoV-2 and SARS-CoV-2 + SSR240612 groups. Interestingly, neither one-way ANOVA nor Tukey's multiple comparison test for percent spontaneous alternation yielded significance.

Nevertheless, the results of percent spontaneous alternation depicted a similar trend of functional recovery observed in total arm entries (Figure 6A-B). The combo group exhibited a similar average percent spontaneous alternation to the mock group, whereas the SARS-CoV-2 infection/vehicle group displayed a decrease. This decline could be associated with a loss in spatial working memory, but it returned to normal with a B1R antagonist. These findings contradict previous findings that have indicated no significant difference in short-term spatial working memory (29). However, it has been found that the hippocampus is especially

susceptible to neuroinflammation, which has been linked to neuroplasticity (30-31). Interestingly, observations of various viral infections, such as influenza and human immunodeficiency virus (HIV), have revealed that abnormal glial cell activation affects hippocampal function (31-34). Thus, our study's findings can be explained by SARS-CoV-2 infection-producing neuroinflammation effects that are being modulated by antagonizing the B1R, as evidenced by the decrease in percent spontaneous alternation in the infected/vehicle group and the subsequent return to normal in the infected/B1R antagonist group.

4.4 Trends Indicate Potential Impact of B1R Antagonist on Anxiety and Exploration

Similarly, all twenty-nine mice underwent behavioral testing, including a zero-maze and open-field test. The zero-maze was previously utilized to measure anxiety levels, while the open field test assessed exploration (12). Zero-maze test results indicate no significant differences between groups' time spent in closed or open areas (Figure 7A-B). Previous research has identified a significant increase in anxiety and depression-like behavior 14 days following viral infection (36). Literature has demonstrated that viral infection can lead to behavioral changes and abnormalities (37). Interestingly, studies have shown that B1R inhibition results in a decrease in anxiety or depressive-like behavior (39). Although the results from our research regarding time spent in open areas were insignificant, by looking at the trends seen in the time spent in closed areas, our study's results comparing infection to sham coincided with those of our laboratory's previously published data, suggesting that SARS-CoV-2 infection increases anxiety-like behavior (12).

In the open field test, no significant difference was found for an alpha level of 0.05 in either the one-way ANOVA or Tukey's multiple comparisons test for rearing or grooming behaviors (Figure 8A-B). However, one-way ANOVA analysis of the total distance traveled

yielded significance (p=0.0001) at the same alpha level with the SARS-CoV-2 infected groups traveling a further average distance (Figure 8C). These findings validate previous results, indicating that overall motor activity was not affected by SARS-CoV-2 infection (12). Due to a statistically significant difference (p=0.0010) between the means of infected groups, it can be concluded that antagonism of the B1R led to improved exploratory behavior. Literature has indicated that exploration could be related to nociception. A recent study examined hypernociception induced by brachial plexus avulsion (BPA). The study found that treatment with SSR240612, a B1R antagonist, significantly reduced mechanical hypernociception induced by BPA (38). Thus, it can be inferred that antagonism of the bradykinin-1 receptor led to decreased neuropathic pain, consequently increasing exploration.

4.5 Mild SARS-CoV-2 Infection Increases B1R Expression

Twenty mice, five per group, were randomly selected for B1R immunostaining. Each mouse brain was harvested and prepared to isolate hippocampal brain structures. Sagittal sections of 10-micron thickness were stained with a B1R antibody.

Quantifying B1R expression yielded statistically significant results (p=0.0448) using a one-way ANOVA with an alpha 0.05. SARS-CoV-2 and SARS-CoV-2 + SSR240612 groups exhibited the highest average receptor expression (Figure 11). These findings corroborate previous results from our lab's published research, demonstrating that SARS-CoV-2 infection increases B1R expression (12). Although Tukey’s multiple comparisons tests did not show significance between the means of the SSR240612 and vehicle groups, a trend suggests decreased B1R expression in the presence of the antagonist. Literature has indicated that increased B1R expression is associated with inflammation; thus, these findings suggest that

SARS-CoV-2 infection may induce inflammation while antagonism of B1R potentially reduces inflammation.

4.6 B1R Antagonism Promotes Microglial Activation

Twenty mice, five in each group, were randomly selected for glial cell immunostaining. Each mouse's brain was harvested and prepared to include the hippocampal region in 10-micron sagittal cuts. The tissue was stained with IBA1 and GFAP for microglia and astrocytes, respectively. A total of two hundred glial cells were analyzed, with fifty cells from each group.

Microglial skeleton analysis yielded statistically significant results ($p < 0.0001$) for the average number of branches using one-way ANOVA with an alpha of 0.05. Tukey's multiple comparisons test revealed a statistically significant difference ($p < 0.0001$) when comparing the means of the combo group against SSR240612. A statistically significant difference ($p=0.0001$) in means was found between the mock and SSR240612 groups.

One-way ANOVA for average branch length also yielded statistical significance ($p=0.0001$) for an alpha of 0.05. Tukey's multiple comparison tests indicated a significant difference ($p<0.0001$) in means between the SARS-CoV-2 infected groups. Similarly, among the sham-treated group, mice treated with B1R antagonist had a significantly higher average number of branches than the vehicle group.

The literature suggests that activated microglia exhibit fewer branches (21) and have shorter processes (39), supporting the conclusion that SARS-CoV-2 infection induces microglial activation. Studies examining the effects of influenza virus have indicated a significant increase in microglial activation in the substantia nigra (39). Thus, it can be inferred that the response to the SARS-CoV-2 virus would be similar, as evidenced by the decrease in branching observed (Figure 10A). Literature investigating the intranasal treatment of the B1R antagonist, R-715, on

Alzheimer's mice found enhanced amyloid beta burden and microglial activation (40). This phenomenon is reflected in the decrease in average branch length observed between SARS-CoV-2 infected groups (Figure 10B)

4.7 B1R Antagonism Opposes SARS-CoV-2 Infection-Induced Astrocyte Activation

Interestingly, one-way ANOVA for astrocyte skeleton analysis revealed similar significant findings to microglia for both the average number of branches ($p<0.0001$) and average branch length ($p<0.0001$). Tukey's test for multiple comparisons showed a significant difference ($p<0.0001$) in the average number of branches in the combo group compared to the virus alone. Tukey's multiple comparisons test for average branch length for astrocytes indicated a significant difference in means between virus alone ($p=0.0244$) and combo ($p=0.0256$) groups compared to the mock. The SARS-CoV-2 group showed the highest average branch length, while the SARS-CoV-2 + SSR240612 group had the lowest average branch length.

Literature suggests that increasing branch length is associated with activated astrocyte morphology (23). Therefore, our findings indicate that SARS-CoV-2 infection induces astrocyte activation, as evidenced by the spike in average branch length. A previous study demonstrated that blocking the B1R reduced astroglial activation induced by focal closed head injury (41). These findings coincide with the results of our study, suggesting that antagonism of the B1R during SARS-CoV-2 infection appears to deactivate astrocytes, as indicated by the decrease in average branch length (Figure 10D).

4.8 Conclusion

In conclusion, our study demonstrates that B1R antagonism influences several factors involved in SARS-CoV-2 infection. We observed a modest 10% improvement in survival among SARS-CoV-2 infected groups in the presence of a B1R antagonist. B1R antagonism led to a

neuroprotective effect for exploratory behavior in the Y-maze test. Similarly, B1R antagonism led to increased exploration despite SARS-CoV-2 infection in the open field test. Contrary to our previous findings, SARS-CoV-2 infection did not cause mice to spend less time in open areas; however, it was found that the mild SARS-CoV-2 infection led to a trend of increasing time spent in closed areas. Our findings also validate previous research indicating that SARS-CoV-2 infection increases B1R expression. Additionally, glial cell analysis indicates glial cell activation during SARS-CoV-2 infection. Nevertheless, it can be concluded that B1R antagonism has the potential to promote microglial activation while mitigating astrocyte activation.

4.9 Limitations/Confounding Variables

A significant area for improvement in the ability to convince correlation of results is the small sample size. In the survival results, it is difficult to say that the SSR240612 treatment significantly improved survival despite seeing a 10% increase due to the same size in each group. Similarly, 50 glial cells were used for skeleton analysis per group when assessing glial cell activation. Despite indicating significant results, additional glial cells are necessary to conclude definitive differences in glial cell activation. The smaller sample size may have also contributed to the difference in zero mazer behavior results from the previous experiment. An additional factor that could have influenced the time spent in open and closed areas in the zero maze is the change in the experimental setup. Mice were given an additional osmotic pump releasing either lipophilic solvent or B1R antagonist, which could have produced heightened trauma to the mice, causing them to stay in the closed areas longer. This could also be seen by the increased time spent in closed areas for control mice compared to the previous experiment.

4.10 Take Away Statement

Overall, our study concludes that the B1R Antagonist SSR240612 plays a role in glial cells' neurological and immune response to inflammation and changes in behavior induced by mild SARS-CoV-2 infection.

5 Chapter 5: References

1. Zhai J, Briese T, Dai E, et al. Real-Time Polymerase Chain Reaction for Detecting SARS Coronavirus, Beijing, 2003. Emerging Infectious Diseases. 2004;10(2):300-303. doi:10.3201/eid1002.030799.

2. World Health Organization. Middle East respiratory syndrome: Global summary and risk assessment - 16 November 2022. World Health Organization. Published 2022. Accessed March 14, 2024. https://www.who.int/publications/i/item/WHO-MERS-RA-2022.1

3. Stokes EK, Zambrano LD, Anderson KN, et al. Coronavirus Disease 2019 Case Surveillance — United States, January 22–May 30, 2020. MMWR Morb Mortal WRep. 2020; 69:759–765. doi:10.15585/mmwr.mm6924e2

4. Chatzis DG, Magounaki K, Pantazopoulos I, Bhaskar SMM. COVID-19 and the cardiovascular system-current knowledge and future perspectives. World J Clin Cases. 2022;10(27):9602–9610. doi:10.12998/wjcc. v10.i27.9602

5. Brodin P. Immune determinants of COVID-19 disease presentation and severity. Nat Med. 2021; 27:28–33. doi:10.1038/s41591-020-01202-8

6. Logue JK, Franko NM, McCulloch DJ, et al. Sequelae in Adults at 6 Months After COVID-19 Infection. JAMA Netw Open. 2021;4: e210830.

7. Vaniprabha A, Logeshwaran J, Kiruthiga T, Shah KB. Examination of the Effects of Long-term COVID-19 Impacts on Patients with Neurological Disabilities Using a Neuro machine Learning Model. BOHR International Journal of Neurology and Neuroscience. 2022;1(1):21-28.

8. Jarrott B, Head R, Pringle KG, Lumbers ER, Martin JH. “LONG COVID”—A hypothesis for understanding the biological basis and pharmacological treatment strategy. Pharmacology Research & Perspectives. 2022;10(1): e00911.

9. Lamers MM, Haagmans BL. SARS-CoV-2 pathogenesis. Nat Rev Microbiol. 2022; 20:270–284. doi:10.1038/s41579-022-00713-0

10. Maury A, Lyoubi A, Peiffer-Smadja N, et al. Neurological manifestations associated with SARS-CoV-2 and other coronaviruses: A narrative review for clinicians. Rev Neurol. 2021;177(1-2):51-64. doi: 10.1016/j.neurol.2020.10.001

11. Albert-Weissenberger C, Stetter C, Meuth SG, et al. Blocking bradykinin receptor, B1 protects from a focal closed-head injury in mice by reducing axonal damage and astroglia activation. J Cereb Blood Flow Metab. 2012;32(9):1747–1756. doi:10.1038/jcbfm.2012.62

12. Sriramula S, Theobald D, Parekh RU, et al. Emerging Role of Kinin B1 Receptor in Persistent Neuroinflammation and Neuropsychiatric Symptoms in Mice Following Recovery from SARS-CoV-2 Infection. Cells. 2023;12(16):2107. doi:10.3390/cells12162107

13. Kwon HS, Koh SH. Neuroinflammation in neurodegenerative disorders: the roles of microglia and astrocytes. Transl Neurodegener. 2020;9(1):42.

14. Garland EF, Hartnell IJ, Boche D. Microglia and Astrocyte Function and Communication: What Do We Know in Humans? Front Neurosci. 2022; 16:824888. doi:10.3389/fnins.2022.824888

15. Hickman S, Izzy S, Sen P, Morsett L, El Khoury J. Microglia in neurodegeneration. Nat Neurosci. 2018; 21:1359–69.

16. Lawson LJ, Perry VH, Dri P, Gordon S. Heterogeneity in the distribution and morphology of microglia in the normal adult mouse brain. Neuroscience.1990;39:151–70.

17. Baufeld C, O'Loughlin E, Calcagno N, Madore C, Butovsky O. J Neural Transm. 2018; 125:809–26.

18. Colombo E, Farina C. Astrocytes: key regulators of neuroinflammation. Trends Immunol. 2016; 37:608–20.

19. Oksanen M, Lehtonen S, Jaronen M, et al. Astrocyte alterations in neurodegenerative pathologies and their modeling in human induced pluripotent stem cell platforms. Cell Mol Life Sci. 2019; 76:2739–60.

20. Walker DG, Lue LF. Immune phenotypes of microglia in human neurodegenerative disease: Challenges to detect microglial polarization in human brains. Alzheimers Res Ther. 2015; 7:56. doi:10.1186/s13195-015-0139-9

21. Leyh J, Paeschke S, Mages B, et al. Classification of microglial morphological phenotypes using machine learning. Front Cell Neurosci. 2021; 15:701673.

22. Carter SF, Herholz K, Rosa-Neto P, Pellerin L, Nordberg A, Zimmer ER. Astrocyte biomarkers in Alzheimer's disease. Trends Mol Med. 2019; 25:77–95.

23. Marques SI, Carmo H, Carvalho F, Sá SI, Silva JP. A Semi-Automatic Method for Quantifying Astrocyte Number and Branching in Bulk Immunohistochemistry Images. Int J Mol Sci. 2023;24(5):4508. doi:10.3390/ijms24054508

24. Olton DS, Branch M, Best PJ. Spatial correlates of hippocampal unit activity. Exp Neurol. 1978;58(3):387-409.

25. Ghafouri S, Fathollahi Y, Javan M, et al. Effect of low-frequency stimulation on impaired spontaneous alternation behavior of kindled rats in Y-maze test. Epilepsy Res. 2016; 126:37-44.

26. de Mello AJ, Moretti M, Rodrigues ALS. SARS-CoV-2 consequences for mental health: Neuroinflammatory pathways linking COVID-19 to anxiety and depression.

27. Lamers MM, Haagmans BL. SARS-CoV-2 pathogenesis. Nat Rev Microbiol. 2022;20:270-284. doi:10.1038/s41579-022-00713-0

28. Hoffmann M, Kleine-Weber H, Schroeder S, et al. SARS-CoV-2 cell entry depends on ACE2 and TMPRSS2 and is blocked by a clinically proven protease inhibitor. Cell. 2020;181(2):271-280.

29. Xu J, Wei H, You P, et al. Non-neutralizing antibodies to SARS-Cov-2-related linear epitopes induce psychotic-like behavior in mice. Front Mol Neurosci. 2023;16:1177961.

30. Barrientos RM, Kitt MM, Watkins LR, Maier SF. Neuroinflammation in the normal aging hippocampus. Neuroscience. 2015;309:84-99.

31. Poluektova L, Meyer V, Walters L, et al. Macrophage-induced inflammation affects hippocampal plasticity and neuronal development in a murine model of HIV-1 encephalitis. Glia. 2005;52(4):344-353.

32. Hosseini S, Wilk E, Michaelsen-Preusse K, et al. Long-term neuroinflammation induced by influenza A virus infection and the impact on hippocampal neuron morphology and function. J Neurosci. 2018;38(12):3060-3080.

33. Jurgens HA, Amancherla K, Johnson RW. Influenza infection induces neuroinflammation, alters hippocampal neuron morphology, and impairs cognition in adult mice. J Neurosci. 2012;32(12):3958-3968.

34. Radhakrishnan RK, Kandasamy M. SARS-CoV-2-mediated neuropathogenesis, deterioration of hippocampal neurogenesis and dementia. Am J Alzheimers Dis Other Demen. 2022;37:15333175221078418.

35. Sriram S, Parekh R, Theobald D, et al. Long COVID in K18-hACE2 mice causes persistent brain inflammation and cognitive impairment.

36. Ge Q, Zhou S, Porras J, et al. SARS-CoV-2 neurotropism-induced anxiety and depression-like behaviors require microglia activation. bioRxiv. 2023-10.

37. Tomonaga K. Virus-induced neurobehavioral disorders: mechanisms and implications. Trends Mol Med. 2004;10:71-77.

38. Quintao NL, Passos GF, Medeiros R, et al. Neuropathic pain-like behavior after brachial plexus avulsion in mice: the relevance of kinin B1 and B2 receptors. J Neurosci. 2008;28(11):2856-2863.

39. Sadasivan S, Zanin M, O'Brien K, Schultz-Cherry S, Smeyne RJ. Induction of microglia activation after infection with the non-neurotropic A/CA/04/2009 H1N1 influenza virus. PLoS One. 2015;10(4):e0124047.

40. Asraf K, Keren N, Torika N, et al. Differential effect of intranasally administrated kinin B1 and B2 receptor antagonists in Alzheimer's disease mice. Biol Chem. 2016;397(4):345-351. doi:10.1515/hsz-2015-0219

41. Albert-Weissenberger C, Stetter C, Meuth SG, et al. Blocking bradykinin receptor, B1 protects from a focal closed-head injury in mice by reducing axonal damage and astroglia activation. J Cereb Blood Flow Metab. 2012;32(9):1747-1756.

42. Jiang P, Yao C, Guo DA. Traditional Chinese medicine for the treatment of immune-related nephropathy: A review. *Acta Pharmaceutica Sinica B*. 2023.

43. Jha MK, Jeon S, Suk K. Glia as a link between neuroinflammation and neuropathic pain. *Immune Network*. 2012;12(2):41-47.

44. Akula, S.M.; Bolin, P.; Cook, P.P. Cellular miR-150-5p may have a crucial role to play in the biology of SARS-CoV-2 infection by regulating nsp10 gene. RNA Biol. 2022, 19, 1-11.

Appendix: IACUC APPROVAL LETTER

ECU

Animal Care and Use Committee
003 Ed Warren Life Sciences Building | East Carolina University | Greenville NC 27834 - 4354
252-744-2436 office | 252-744-2355 fax

November 19, 2020

Jeffrey Eells, Ph.D.
Department of Anatomy and Cell Biology, ECU

Dear Dr. Eells:

Your Animal Use Protocol entitled, "Effects of COVID-19 on dopamine neuron survival" (AUP #A209) was reviewed by this institution's Animal Care and Use Committee on 11/19/2020. The following action was taken by the Committee:

"Approved as submitted"

****Please contact Aaron Hinkle prior to any hazard use****

A copy of the protocols is enclosed for your laboratory files. Please be reminded that all animal procedures must be conducted as described in the approved Animal Use Protocol. Modifications of these procedures cannot be performed without prior approval of the ACUC. The Animal Welfare Act and Public Health Service Guidelines require the ACUC to suspend activities not in accordance with approved procedures and report such activities to the responsible University Official (Vice Chancellor for Health Sciences or Vice Chancellor for Academic Affairs) and appropriate federal Agencies. **Please ensure that all personnel associated with this protocol have access to this approved copy of the AUP/Amendment and are familiar with its contents.**

Sincerely yours,

Susan McRae, Ph.D.
Chair, Animal Care and Use Committee

SM/GD

enclosure

Animal Care and Use Committee
003 Ed Warren Life Sciences Building | East Carolina University | Greenville NC 27834 - 4354
252-744-2436 office | 252-744-2355 fax

January 26, 2023

Jeffrey Eells, Ph.D.
Department of Anatomy and Cell Biology, ECU

Subject: Protocol A209, original approval date 11/19/2020

Dear Dr. Eells:

The amendment#5 to your Animal Use Protocol entitled, "Effects of COVID-19 on dopamine neuron survival" (AUP#A209) was reviewed by this institution's Animal Care and Use Committee on 1/25/2023. The following action was taken by the Committee:

"Approved as submitted"

Please contact Aaron Hinkle prior to any hazard use

A copy of the protocols is enclosed for your laboratory files. Please be reminded that all animal procedures must be conducted as described in the approved Animal Use Protocol. Modifications of these procedures cannot be performed without prior approval of the ACUC. The Animal Welfare Act and Public Health Service Guidelines require the ACUC to suspend activities not in accordance with approved procedures and report such activities to the responsible University Official (Vice Chancellor for Health Sciences or Vice Chancellor for Academic Affairs) and appropriate federal Agencies. Please ensure that all personnel associated with this protocol have access to this approved copy of the AUP/Amendment and are familiar with its contents.

Sincerely yours,

Sue McRae, Ph.D. Chair, Animal Care and Use Committee

SM/GD

enclosure